Model Comparisons Between Canonical Vine Copulas and Meta-Gaussian for Forecasting Agricultural Drought over China

Authors: Haijiang Wu[1,2], Xiaoling Su[1,2*], Vijay P. Singh[3,4], Te Zhang[2], Jixia Qi[2], and Shengzhi Huang[5]

Affiliation:

[1]*Key Laboratory for Agricultural Soil and Water Engineering in Arid Area of Ministry of Education, Northwest A&F University, Yangling, Shaanxi, 712100, China*

[2]*College of Water Resources and Architectural Engineering, Northwest A&F University, Yangling, Shaanxi, 712100, China*

[3]*Department of Biological and Agricultural Engineering & Zachry Department of Civil and Environmental Engineering, Texas A&M University, College Station, TX 77843-2117, USA*

[4]*National Water and Energy Center, UAE University, Al Ain, UAE*

[5]*State Key Laboratory Base of Eco-Hydraulic Engineering in Arid Area, Xi'an University of Technology, Xi'an, Shaanxi, 710048, China*

*Corresponding Author:

Dr. Xiaoling Su, College of Water Resources and Architectural Engineering, Northwest A&F University, Weihui Road 23, Yangling, Shaanxi, China, *Email*: xiaolingsu@nwafu.edu.cn (X. Su).

Abstract

Agricultural drought is mainly caused by reduced soil moisture and precipitation and shows adverse impacts on the growth of crops and vegetation, thus affecting agricultural production and food security. For developing measures for drought mitigation, reliable agricultural drought forecasting is essential. In this study, we developed an agricultural drought forecasting model based on canonical vine copulas under three-dimensions (3C-vine model), in which the antecedent meteorological drought and agricultural drought persistence were utilized as predictors. Besides, the meta-Gaussian (MG) model was selected as a reference model to evaluate the forecast skill. The agricultural drought in August of 2018 was selected as a typical case study, and the spatial patterns of 1–3-month lead forecasts of agricultural drought utilizing the 3C-vine model resembled the corresponding observations, indicating the good predictive ability of the model. The performance metrics (NSE, R^2, and RMSE) showed that the 3C-vine model outperformed the MG model for forecasting agricultural drought in August under diverse lead times. Also, the 3C-vine model exhibited excellent forecast skills in capturing the extreme agricultural drought over different selected typical regions. This study may help to guide drought early warning, drought mitigation, and water resources scheduling.

Keywords: drought forecasting, model comparison, vine copulas, meta-Gaussian

1. Introduction

Agriculture is the source of livelihoods of over 2.5 billion people worldwide, and the agricultural sector also sustains 82% of all drought impacts (FAO, 2021). A cascade of impacts of droughts, such as crop reduction and failure, increased human and tree mortality, and ecological disturbance, have attracted considerable attention (FAO, 2021; Lu et al., 2012; Modanesi et al., 2020;

Su et al., 2018; Zhang et al., 2018; Zhang et al., 2019; Zscheischler et al., 2020). Droughts have reduced global crop production by about 9–10% for the period 1964–2007 (Lesk et al., 2016). Additionally, droughts have caused overall crop and livestock production loss of $37 billion over the least developed and lower-middle-income countries (FAO, 2021). Agricultural drought forecasting, therefore, lies at the core of overall drought risk management and is critical for food security, early warning, as well as drought preparedness and mitigation.

Agricultural drought is generally referred to as soil moisture shortage, which adversely affects crop yield and vegetation health (Modanesi et al., 2020; Zhang et al., 2016; Zhang et al., 2021). Under natural conditions, atmospheric precipitation is a paramount source for replenishment of soil moisture (Wu et al., 2021a). Therefore, reduced soil moisture (agricultural drought) mainly arise from precipitation deficit (meteorological drought) (Modanesi et al., 2020; Orth and Destouni, 2018). Moreover, soil moisture has a good memory to drought because of the time-integration effects (Long et al., 2019), i.e., agricultural drought persistence. Previous meteorological drought and antecedent agricultural drought can be taken into consideration as predictors of subsequent agricultural drought.

In hydrology, some physically-based hydrological models (e.g., Distributed Time-Variant Gain Hydrological Model (DTVGM; Ma et al, 2021) and Soil and Water Assessment Tool (SWAT; Wu et al., 2019)) are widely used in hydrological simulation and prediction, the droughts included as well. However, the physically-based hydrological models typically apply to a catchment or sub-regional scale, and generally require numerous hydrometeorological variables to achieve more accurate real-time predictions (Liu et al., 2021a; Xu et al., 2021a). Traditional methods, such as regression models, machine learning models, and hybrid models (by considering both statistical and dynamical predictions) (Hao et al., 2016), have been extensively employed to forecast drought. Yet, these models tend to be limited in considering the complex nonlinear (e.g., regression models), explicit physical mechanisms and over-fitting (e.g., machine learning models), as well as the demand of massive hydroclimatic data input (e.g., hybrid models). The copula functions overcome the limitations of aforementioned conventional statistical methods. Since copulas are flexible joining arbitrary marginal distributions of variables, they have been widely employed in risk assessment (Hao et al., 2017; Liu et al., 2021b; Sarhadi et al., 2016; Xu et al., 2021b; Zhang et al., 2021; Zhou et al., 2019), flood and runoff forecasting (Bevacqua et al., 2017b; Hemri et al., 2015; Liu et al., 2018; Zhang and Singh, 2019), and drought forecasting (Ganguli and Reddy, 2014; Wu et al., 2021a). However, when bivariate copulas are extended to higher-dimensional (≥ three-dimensions) cases, they are restricted due to nonexistence of analytical expressions (Liu et al., 2021a). Symmetric Archimedean copulas and nested Archimedean copulas partially have addressed the issues of dimensionality, but single parameter and Archimedean class are difficult to characterize the various dependence structures (Aas and Berg, 2009; Hao et al., 2016; Wu et al., 2021a). Fortunately, the vine copulas addressed these limitations (Aas et al., 2009; Bedford and Cooke, 2002; Joe, 1996).

Vine copulas are flexible in decomposing any multi-dimensional joint distribution into a hierarchy of bivariate copulas or pair copula constructions (Aas et al., 2009; Bedford and Cooke, 2002; Liu et al., 2021a; Vernieuwe et al., 2015; Xiong et al., 2014). These copulas have been extensively applied in the hydrological field (Bevacqua et al., 2017b; Liu et al., 2021b; Vernieuwe et al., 2015; Wu et al., 2021a). For instance, Xiong et al. (2014) derived the annual runoff distributions using canonical vine copulas. Liu et al. (2018) developed a framework to investigate compound floods based on canonical vine copulas. Wang et al. (2019) utilized regular vine copulas with historical streamflow and climate drivers to simulate monthly streamflow for the headwater catchment of the Yellow River basin. Liu et al. (2021a) developed a hybrid ensemble forecast model, using the Bayesian model averaging combined canonical vine copulas, to forecast water level. Wu et al. (2021a) proposed an agricultural drought forecast model based on vine copulas under four-dimensional scenarios.

The meta-Gaussian (MG) model, a popular statistical model in the hydrometeorological community, has explicit conditional distributions, which is apt for forecasting and risk assessment purposes (Hao et al., 2016; Hao et al., 2019a; Wu et al., 2021b; Zhang et al., 2021). The forecast skills of the MG model for drought or compound dry-hot events, for example, outperformed the persistence-based or random forecast models (Hao et al., 2016; Hao et al., 2019a; Wu et al., 2021b). However, the MG model only depicts the linear relationship among explanatory variables (predictors) and forecasted variable via covariate matrix, it cannot characterize the nonlinear or tail dependence existing in the variables (Hao et al., 2016). Fortunately, Vine copulas can flexibly combine multiple variables via bivariate copula to characterize numerous or complex dependencies. There has been a rather limited investigation, to our knowledge, that conducting model comparisons between vine copulas and MG for agricultural drought forecasting under the same conditions. Therefore, investigations on drought forecasting skills between vine copulas and the MG model are needed to obtain more reliable drought forecasts.

The objective of this study therefore was to compare the forecast ability of agricultural drought in August of every year in the period 1961–2018 between canonical vine copulas (i.e., 3C-vine model) and MG model under three-dimensional scenario. In the following, we briefly describe the study area and data used in Section 2. The MG and 3C-vine models and performance metrics utilized are presented in Section 3. Results of the 3C-vine model application and assessment are displayed in Section 4. Finally, the discussion and conclusions are presented in Section 5.

2. Study area and data used

China stretches across a vast area covering diverse climate regimes and is a major agricultural-producing country (Wu et al., 2021a; Zhang et al., 2015). For the convenience of analyzing spatial patterns of agricultural drought, the climate of China was divided into seven sub-climate regions on the basis of Zhao (1983) and Yao et al. (2018), as shown in Figure 1. For each sub-climate region, the temperature and moisture conditions when combined are roughly similar, and the type of soil and vegetation have a certain common characteristic (Zhao, 1983).

--Figure 1. ---

In this study, the gridded monthly precipitation with a 0.25°×0.25° spatial resolution was obtained from the CN05.1 dataset for the 1961–2018 period over the mainland of China (excluding the Taiwan province), which was provided by the China National Climate Center. The Copernicus Climate Change Service (C3S) at European Center for Medium-Range Weather Forecast (ECMWF) has begun the release of the ERA5 back extension data covering the period 1950–1978 on the Climate Data Store (CDS). Therefore, the gridded monthly soil moisture with a 0.25°×0.25° spatial resolution corresponding to three soil depths (0–7 cm, 7–28 cm, and 28–100 cm) are available from the ECMWF ERA5 reanalysis datasets for 1961–1978: https://cds.climate.copernicus.eu/cdsapp#!/dataset/reanalysis-era5-single-levels-monthly-means-preliminary-back-extension?tab=overview and 1979–2018: https://cds.climate.copernicus.eu./cdsapp#!/dataset/reanalysis-era5-single-levels-monthly-means?tab=overview. The CN05.1 and ERA5 reanalysis datasets have been extensively utilized numerous studies, e.g., drought monitoring and forecasting (Wu et al., 2021a; Zhang et al., 2021), long-term climatic analysis (He et al., 2021; Wu et al., 2017), and flash drought attribution analysis (Wang and Yuan, 2021).

3. Methodology

The Standardized Precipitation Index (SPI, based on monthly precipitation) and Standardized Soil moisture Index (SSI, based on monthly cumulative soil moisture at top-three soil depths) is leveraged to characterize meteorological drought and agricultural drought at a 6-month timescale, respectively. The empirical Gringorten plotting position formula (Gringorten, 1963) was used to obtain the empirical cumulative probabilities of these two indexes, which were then transformed into standardized variables via the normal quantile transformation. Since meteorological drought is a source of other drought types (e.g., agricultural drought), the antecedent precipitation deficiency (i.e., meteorological drought) has a stronger effect on the subsequent soil moisture deficiency (i.e., agricultural drought). Moreover, soil moisture has a good memory for prior drought, i.e., agricultural drought persistence, which is attributed to the soil porosity characteristics and time-integration effects (Long et al., 2019; Wu et al., 2021a).

We attempted to use the prior meteorological drought (SPI_{t-i}; t denotes the target month (e.g., August), and i indicates lead time (month)) and agricultural drought persistence (SSI_{t-i}) to forecast the subsequent agricultural drought (SSI_t) based on the canonical vine copulas under three-dimensional scenarios (3C-vine model). We selected the meta-Gaussian (MG) model as a reference model to assess the agricultural drought forecast performance of the 3C-vine model. Here, the 6-month timescale SPI (SSI) in August, which is calculated by the cumulative precipitation (soil moisture) from March to August, can indirectly reflect the surplus or deficit situations of water in spring (March-April-May) and summer (June-July-August) seasons. Furthermore, August is a key growth period for crops (e.g., anthesis, fruiting, and seed filling) and vegetation and is also a period with frequent droughts (Wu et al., 2021a). Undoubtedly, agricultural drought forecast can be implemented in any month of interest, based on 3C-vine model and MG model. More detailed information is given below.

3.1. Meta-Gaussian model under three-dimensional scenarios

Meta-Gaussian (MG) model can effectively combine multiple hydrometeorological variables, which have gained attention for drought forecasting and risk assessment (Hao et al., 2019a; Hao et al., 2019b; Wu et al., 2021b; Zhang et al., 2021). Suppose the series of SPI_{t-i}, SSI_{t-i}, and SSI_t correspond to random variables Y_1, Y_2, and Y_3, respectively, the predictand y_3 under the given conditions of y_1 and y_2 based on the MG model can be expressed as (Wilks, 2014):

$$y_3 \mid (y_1, y_2) \sim N(\mu_{y_3|(y_1,\, y_2)}, \Sigma_{y_3|(y_1,\, y_2)}) \tag{1}$$

where N signifies the Gaussian distribution function; $\mu_{y_3|(y_1,\, y_2)}$ denotes the conditional mean; and $\Sigma_{y_3|(y_1,\, y_2)}$ represents the conditional covariate matrix.

Furthermore, we removed the forecast values in a specific year of y_1, y_2, and y_3, which denote y_1^{-yr}, y_2^{-yr}, and y_3^{-yr}, respectively. Under this circumstance, the covariate matrix $\mathbf{\Sigma}$ regarding y_1^{-yr}, y_2^{-yr}, and y_3^{-yr} can be written as:

$$\mathbf{\Sigma} = Cov\left[\begin{array}{cc|c} (y_1^{-yr}, y_1^{-yr}) & (y_1^{-yr}, y_2^{-yr}) & (y_1^{-yr}, y_3^{-yr}) \\ (y_2^{-yr}, y_1^{-yr}) & (y_2^{-yr}, y_2^{-yr}) & (y_2^{-yr}, y_3^{-yr}) \\ \hline (y_3^{-yr}, y_1^{-yr}) & (y_3^{-yr}, y_2^{-yr}) & (y_3^{-yr}, y_3^{-yr}) \end{array}\right] = \left[\begin{array}{cc|c} C_{11} & C_{12} & C_{13} \\ C_{21} & C_{22} & C_{23} \\ \hline C_{31} & C_{32} & C_{33} \end{array}\right] = \begin{bmatrix} \mathbf{\Sigma}_{11} & \mathbf{\Sigma}_{12} \\ \mathbf{\Sigma}_{21} & \mathbf{\Sigma}_{22} \end{bmatrix} \tag{2}$$

The forecast of specific years, i.e., y_3^{yr}, can be derived as (Wilks, 2014):

$$y_3^{yr} = \mu_{y_3^{-yr}} + \mathbf{\Sigma}_{21}\mathbf{\Sigma}_{11}^{-1}\begin{bmatrix} y_1^{yr} - \mu_{y_1^{-yr}} \\ y_2^{yr} - \mu_{y_2^{-yr}} \end{bmatrix} \tag{3}$$

where $\mu_{y_1^{-yr}}$, $\mu_{y_2^{-yr}}$, and $\mu_{y_3^{-yr}}$ represent the mean of y_1^{-yr}, y_2^{-yr}, and y_3^{-yr}, respectively; y_1^{yr} and y_2^{yr} denote that y_1 and y_2 provided the forecast information at time $t–i$ in a specific year. More details about forecasting agricultural drought based on the MG model can be found in Figure 3.

3.2. Canonical vine copulas model under three-dimensional scenarios

Copulas can effectively combine multiple variables without the restriction of marginal distributions (Nelsen, 2013; Sarhadi et al., 2016; Wang et al., 2019; Xiong et al., 2014). They were initially utilized for deriving joint distributions of two-dimensional variables, since parameters are easy to assess and the analytical solution is apt to obtain (Liu et al., 2021a; Sadegh et al., 2017). However, under higher-dimensional (e.g., $d \geqslant 3$) scenarios, owing to the limitations of a great deal of parameters and complexity, the copulas (mainly referred to bivariate copulas) are difficult to promote and apply (Joe, 2014; Liu et al., 2018; Liu et al., 2021a; Sadegh et al., 2017). To overcome these limitations, Joe (1996) and Aas et al. (2009) developed vine copulas, a hierarchy of pair copula constructions, for multi-dimensional cases. Vine copulas possess two sub-classes: canonical vine copulas (C-vine copulas) and drawable vine copulas (D-vine copulas). Here, we mainly employed the C-vine copulas to establish the forecast model of agricultural drought under three-dimensional conditions. Undoubtedly, a similar scheme is capable of applying to D-vine copulas.

C-vine copulas may have numerous tree structures, especially for the case of higher dimensions, which are associated with the quantity and ordering of variables (Aas et al., 2009; Liu et al., 2018; Liu et al., 2021a; Wu et al., 2021a). Also, different ordering of variables affects the estimation of the parameters of C-vine copulas (Liu et al., 2021a; Wang et al., 2019). Given the ordering of variables

Y_1, Y_2, and Y_3 for three-dimensional C-vine copula model (termed as 3C-vine model hereinafter; Figure 2a), the joint probability density function (PDF), g_{123}, can be expressed as (Aas et al., 2009):

$$g_{123} = g_1 \bullet g_2 \bullet g_3 \bullet c_{12} \bullet c_{13} \bullet c_{23|1} \tag{4}$$

where g_1, g_2, and g_3 correspond to the margin density functions of $g_1(y_1)$, $g_2(y_2)$, and $g_3(y_3)$, respectively; c is the bivariate copula density; c_{12}, c_{13}, and $c_{23|1}$ signify the abbreviation of $c_{1,2}[G_1(y_1), G_2(y_2)]$, $c_{1,3}[G_1(y_1), G_3(y_3)]$, and $c_{2,3|1}[G(y_2|y_1), G(y_3|y_1)]$, respectively. The Gaussian (or Normal), Student-t, Clayton, and Frank copulas, as well as their rotated (survival) forms (Dißmann et al., 2013; Liu et al., 2021b) are utilized to obtain the optimal internal bivariate copulas for distinct trees in 3C-vine models based on the Akaike information criterion (AIC). With the help of *CDVineCondFit* R function in "*CDVineCopulaConditional*" R package (Bevacqua, 2017a), based on the AIC, we selected the optimal tree structures (i.e., detected the suitable variable ordering; seen in Figure 2).

--Figure 2. --

A conditional copula density needs to be addressed in Equation 4, i.e., $G(y|\mathbf{w})$, where $\mathbf{w}$ is a d-dimensional vector $\mathbf{w} = (w_1, \ldots, w_d)$. Here, regarding the conditional distribution of y given the conditions $\mathbf{w}$, we introduced the h-function, $h(y, \mathbf{w}; \theta)$, to indicate the $G(y|\mathbf{w})$ as follows (Aas et al., 2009; Joe, 1996):

$$h(y,\mathbf{w};\theta) := G(y\,|\,\mathbf{w}) = \frac{\partial C_{y,w_j|\mathbf{w}_{-j}}\left[G(y\,|\,\mathbf{w}_{-j}), G(w_j\,|\,\mathbf{w}_{-j})\right]}{\partial G(w_j\,|\,\mathbf{w}_{-j})} \tag{5}$$

where θ denotes the parameter(s) of bivariate copula function $C_{yw_j|\mathbf{w}_{-j}}$; w_j represents an arbitrary component of $\mathbf{w}$; and w_{-j} indicates the excluding element w_j from the vector $\mathbf{w}$.

Let the ordering variables be y_1, y_2, and y_3, the conditional variables be y_1 and y_2, and the predictand be y_3. Accordingly, the expression of $G(y_3|y_1, y_2)$, based on Equation 5, can be written as:

$$G(y_3 \mid y_1, y_2) = \frac{\partial C_{z_3, z_1|z_2}\left[G(y_3 \mid y_1), G(y_2 \mid y_1)\right]}{\partial G(y_2 \mid y_1)} = h\left\{h(u_3 \left|u_1; \theta_{12}\right.) \left| h(u_2 \left|u_1; \theta_{11}\right.); \theta_{21}\right.\right\} \tag{6}$$

where θ_{ij} (i denotes a tree and j is an edge) represents the parameters of different conditional copulas in the 3C-vine model (Figure 2a); and u_k (k = 1, …, 3) is the marginal cumulative distribution function (CDF) of y_k. The CDF for each variable is substituted by the corresponding empirical Gringorten cumulative probability (Bevacqua et al., 2017b; Genest et al., 2009; Wu et al., 2021a).

Here, we introduced the τ-th copula–quantile curve (Chen et al., 2009; Liu et al., 2018) to simulate u_3 based on Equation 6 and derived its inverse distribution function as follows:

$$y_3 = N^{-1}\left\{G(\tau \mid z_1, z_2)\right\} = N^{-1}(u_3) = N^{-1}\left[h^{-1}\left\{h^{-1}(\tau \left| h(u_2 \left|u_1; \theta_{11}\right.); \theta_{21}\right.) \left|u_1; \theta_{12}\right.\right\}\right] \tag{7}$$

where N^{-1} and h^{-1} signify the inverse form of Gaussian distribution and h-function, respectively; y_3 is the forecasted agricultural drought at time t (i.e., SSI_t); y_1 and y_2 are the predictors corresponding to the antecedent meteorological drought and agricultural drought persistence at time $t–i$ (i.e., SPI_{t-i} and SSI_{t-i}). The R functions of *BiCopHfunc* and *BiCopHinv* in the R package "*VineCopula*" (Nagler et al., 2021) were utilized to model the h-function and its inverse form for Equation 7, respectively.

The tree structure is related to the ordering variables, so when the ordering variables are y_2, y_1, and y_3 (conditional variables are y_1 and y_2; Figure 2b), Equations 6 and 7 can be changed analogously as:

$$G(y_3 \left|y_2, y_1\right.) = h\left\{h(u_3 \left|u_2; \theta_{12}\right.) \left| h(u_1 \left|u_2; \theta_{11}\right.); \theta_{21}\right.\right\} \tag{8}$$

$$y_3 = N^{-1}(u_3) = N^{-1}\left[h^{-1}\left\{h^{-1}(\tau \left| h(u_1 \left|u_2; \theta_{11}\right.); \theta_{21}\right.) \left|u_2; \theta_{12}\right.\right\}\right] \tag{9}$$

With agricultural drought forecast via 3C-vine model, as the details presented in Figure 3, we first selected the best 3C-vine model (i.e., selected the best model from Equations 7 and 9 according to AIC). Then, a sample size of 1,000 uniformly distributed random values was generated over the interval [0, 1] by Monte Carlo simulation. Last, the best 3C-vine model was utilized to obtain 1,000 simulations (or estimations) for y_3^{yr}. The best forecast of y_3^{yr} was finally calculated by the mean value of these simulations. Note that the leave-one-out cross validation (LOOCV) (Wilks, 2014) is applied to forecast agricultural drought for each grid cell in August of every year during 1961–2018 based on the 3C-vine or MG models, namely, each time one sample (or observation) was left for validation, and the rest were used to establish 3C-vine model or MG model and obtain the corresponding parameters of these models. In other words, this process was repeated 58 times (the length of years used in this study) for a specific grid cell.

--Figure 3. ---

3.3. Performance metrics

Three evaluation metrics: Nash-Sutcliffe efficiency (NSE), coefficient of determination (R^2), and root mean square error (RMSE), were utilized to assess the forecast performance of 3C-vine model and MG model. These metrics can be expressed as:

$$NSE = 1 - \frac{\sum_{i=1}^{n}(AP_i - AO_i)^2}{\sum_{i=1}^{n}(AO_i - \overline{AO})^2} \qquad NSE \in (-\infty, 1] \tag{10}$$

$$R^2 = \frac{\left[\sum_{i=1}^{n}(AO_i - \overline{AO})(AP_i - \overline{AP})\right]^2}{\sum_{i=1}^{n}(AO_i - \overline{AO})^2 \bullet \sum_{i=1}^{n}(AP_i - \overline{AP})^2} \qquad R^2 \in [0,1] \tag{11}$$

$$RMSE = \sqrt{\frac{1}{n}\sum_{i=1}^{n}(AP_i - AO_i)^2} \qquad RMSE \in [0, +\infty) \tag{12}$$

where n is the number of forecast periods; AO_i and AP_i are the i-th observed and forecasted agricultural droughts (i.e., SSI), respectively; $\overline{AO}$ and $\overline{AP}$ denote the mean of the SSI observations and forecasts in the target month (e.g., August), respectively. Moreover, a most positive NSE and R^2 value and a lower RMSE value indicate a good forecast performance for the 3C-vine model or MG model.

4. Results

4.1. Correlation patterns of agricultural drought with potential predictors

The dependence between variables can be measured by the correlation coefficient, indirectly characterizing the quantity of common information between two variables. We employed Kendall's correlation coefficient (τ_k) to measure the dependence of agricultural drought at current time t (SSI_t, herein t is August) with the previous meteorological drought (SPI_{t-i}, i indicates the lag or lead time with 1–3-month herein) and agricultural drought persistence (SSI_{t-i}). It should be mentioned that the significant correlation prevalent used may overestimate or overinterpret the dependence between variables (Wilks, 2016). Therefore, we adopted the maximum false discovery rate (FDR) of 0.1 to correct τ_k at the 0.05 significance level (Benjamini and Hochberg, 1995; Röthlisberger and Martius, 2019; Wilks, 2016).

---Figure 4. ---

Figure 4 summarizes 1–3-month lag τ_k between antecedent SPI (SSI) and succedent SSI for August during 1961–2018 over China. For most regions of China under 1–3-month lag times, the previous meteorological drought or agricultural drought persistence (memory) showed significant positive correlations (i.e., the stippling in Figure 4) with the target agricultural drought. Also, we found perfect agricultural drought memory over many regions of China (excluding D4, a humid climate region) (Figures 4e and 4f), as the overlapping information existed in SSI_t and SSI_{t-i}. Additionally, the dependency pattern varied temporally and spatially, and this phenomenon evidently occurred with the lag (or lead) time extended, especially between SPI_{t-i} and SSI_t (Figures 4a–4c). Overall, the prior meteorological drought and agricultural drought memory provided reliable and useful forecast information for the subsequent agricultural drought for most areas of China.

4.2. Forecast performance comparison between 3C-vine model and MG Model

We leveraged the MG model as a reference model to measure the performance of 3C-vine model in forecasting agricultural drought for the period 1961–2018 over China. Figures 5a–5i show the difference in *NSE*, R^2, and *RMSE* between 3C-vine and MG models, i.e., $\Delta NSE = NSE_{3C} - NSE_{MG}$, $\Delta R^2 = R^2_{3C} - R^2_{MG}$, and $\Delta RMSE = RMSE_{3C} - RMSE_{MG}$ under 1–3-month lead times for August, respectively. In terms of the spatial extent of $\Delta NSE > 0$, $\Delta R^2 > 0$, and $\Delta RMSE < 0$, the agricultural drought forecast ability of 3C-vine model superior MG model was occupied 65%, 68%, and 58% of land areas in China, respectively, under the 1-month lead SSI forecast (Figures 5a, 5d, and 5g). The relationship between predictors and the forecasted variable was simple under 1–month lead time, so the MG model better showed their connection. However, with the lead time prolonged, the forecast skills of 3C-vine model outperformed the MG model for most regions of China (e.g., Figures 5e and 5f, accounting 72% and 74% of land areas in China for $\Delta R^2 > 0$ under 2–3-month lead times, respectively). This indicates the 3C-vine model sufficiently utilized the forecasted information contained by previous meteorological drought and agricultural drought persistence in comparison with the MG model under the same conditions.

The forecast ability of 3C-vine model, compared with the MG model, is limited over climate region D5 (e.g., Figures 5b and 5c). This may be related to the fact that D5 is a crucial grain-producing region in China (Lu et al., 2012; Xiao et al., 2019; Zhang et al., 2016), the intensive anthropogenic activities (e.g., irrigation and urbanization) may alter the linkage between meteorological drought and agricultural drought, as well as the strength of agricultural drought memory (AghaKouchak et al., 2021). To ensure food security, if D5 experiences a drought event at the previous stage, agricultural managers and policymakers would mitigate the drought through irrigation in a variety of ways, such as groundwater exploitation and reservoir operation (Zhang et al., 2016). However, under this circumstance, the soil water obtaining the supplement from the irrigation water would affect the performance of agricultural drought forecast.

---Figure 5. ---

In contrast with the MG model, the 3C-vine model yielded a better forecast performance for August under 1–3-month leads agricultural drought across most areas of China, except for the climate region D5.

4.3. Case study and sub-climate region assessment

The severe drought hit most regions of China in summer 2018, especially in southern and northern China, as the western North Pacific subtropical high abnormally impacted (Liu and Zhu, 2019; Zhang et al., 2020; Zhang et al., 2018). We chose the agricultural drought that occurred in August of 2018 as a case study to investigate the forecast ability of 3C-vine model. Similarly, the MG model was selected as a benchmark model. Figure 6 presents the SSI observations and 1–3-month lead SSI forecasts for this agricultural drought using the 3C-vine model and MG model. Obviously, the 1–3-month lead SSI forecasts via 3C-vine model resembled the observations (Figures 6a–6d), which captured the droughts that emerged in southern China, northern China, and northeastern China, i.e., climate regions D1–D2 and D4–D6. Comparing the 3C-vine model with the MG model under 2–3-month leads (Figures 6c–6d versus Figures 6f–6g), we observed the deteriorating forecast skill of MG model in climate region D5, which tended to non-drought state (i.e., SSI > 0), but the 3C-vine model better forecasted the agricultural drought for these regions under the same conditions, although the severity of agricultural drought had some decrement. The above analyses indicated that the 3C-vine model, using previous meteorological drought and agricultural drought persistence as two predictors, had the ability for reliable drought forecast over many regions of China.

--Figure 6. --

--Figure 7. --

Furthermore, to explore the skill of 3C-vine model in capturing the extremum of agricultural drought (i.e., minimum and maximum SSIs), we randomly selected a typical region (black rectangle boxes in Figure 6b) in each climate region. Note that these extreme SSI values were calculated using the spatial average in each typical region. Figures 7a and 7b shows the probability density function (PDF) curve of minimum and maximum SSIs for these selected typical regions (D1S–D7S) via the 3C-vine model and MG model for 1–3-month leads of August. Here, the vertical black dash line denotes the SSI observation in each subplot. The *x*-axis value of peak point (i.e., high probability) for each PDF curve is regarded as the best estimation of SSI under diverse lead times. With the 3C-vine model as an example (analogously for the MG model), for minimum SSI with 1–2-month lead times, the difference between forecasted SSI and observed SSI was slight (except for D3S), which all reflected the drought state for these typical regions (Figure 7a). The deteriorated skills of 3C-vine and MG models in a typical region D3S may be attributed to the lengthy response time existing between precipitation deficiency and soil moisture shortage, which is caused by the limited precipitation that cannot effectively replenish the soil moisture depletion due to the incrassation of vadose zone. For the 3-month lead time, the poor forecasts were produced in a typical region D5S for the minimum SSI. This phenomenon may result in the agricultural manager utilizing irrigation to mitigate the effect of drought on crop growth, thus, the response relationship between meteorological drought and agricultural drought accordingly would change (Xu et al., 2021b).

For the forecasted maximum SSI utilizing 3C-vine model (analogously for the MG model) over diverse regions, the excellence forecast ability is displayed for the 1–3-month leads (Figure 7b), excluding the typical regions D5S and D6S (PDF curve shifted left). For the abundant precipitation and higher soil moisture content in D6S, the shortened response time between precipitation and soil moisture (Xu et al., 2021b) may cause inferior forecasts of 3C-vine model for the target month.

To display the robustness of 3C-vine model for forecasting agricultural drought in any month of interest, we further forecasted extreme agricultural drought in July for D1S–D7S (Figures 7c and 7d). The difference between forecasted and observed extreme SSIs for the MG model is larger than that of 3C-vine model in distinct typical regions, e.g., the forecasted maximum SSI in July on D4S (Figure 7d). The width of PDF curve qualitatively provides an estimation of forecast uncertainty of 3C-vine model and MG model. As shown in Figure 7, in comparison with the 3C-vine model, we found that the width of PDF curves in the MG model are broadened, indicating that the MG model produced more pronounced uncertainty for agricultural drought forecast. Furthermore, the skills of MG model tended to deteriorate over many selected typical regions, especially for 2–3-month lead times of July and August. Generally, compared with the MG model under different lead times, agricultural drought forecasts made by the 3C-vine model are more accurate across different typical regions, in terms of predictive uncertainty (i.e., the width of PDF curve) as well as the difference between observed and forecasted extreme SSIs (Figures 7).

Moreover, to assess the forecast performance (according to *NSE*, R^2, and *RMSE*) of the 3C-vine model over each climate region, we counted the pixel contained in each climate region and constructed the boxplots for these performance metrics (Figures 5j–5l). We still selected the MG model as the reference model, and obtained the difference between these two models, i.e., ΔNSE, ΔR^2, and $\Delta RMSE$. The forecast performances of 3C-vine model and MG model were generally consistent for 1-month lead of August over climate regions D1–D7 (Figures 5j–5l, the median percentile of ΔNSE, ΔR^2, and $\Delta RMSE$ were all around the 0 line), indicating the improved skills of 3C-vine model was limited under the same condition. Obviously, the median percentile of ΔNSE and ΔR^2 were greater than 0 as well as $\Delta RMSE$ was lower than 0, respectively, for 2–3-month leads SSI forecast of August in different climate regions D1–D7 (except for D5), indicating that the 3C-vine model shows a better performance than the MG model in forecasting agricultural drought over diverse climate regions of China.

In conclusion, based the ability of typical agricultural drought forecasted (Figure 6) and extremum agricultural drought captured in selected typical regions (Figure 7) and the comprehensive forecast performance showed in diverse climate regions (Figures 5j–5l), the 3C-vine model had a good forecast skill for 1–3-month leads agricultural drought of August over most areas of China.

5. Discussion and Conclusions

This study developed a C-vine copula model for forecasting agricultural drought over China under three dimensions, in which antecedent meteorological drought and agricultural drought persistence were employed as two predictors. We selected the MG model as a competition model, in terms of the difference in NSE, R^2, and RMSE between 3C-vine and MG models, to evaluate the forecast performance of 3C-vine model. These performance metrics all displayed that the 3C-vine model, especially for 2–3-month lead times, outperformed the MG model in many climate regions over China (except for D5, which lies in humid and subhumid regions of northern China) (Figure 5). Compared with the MG model, the 3C-vine model yielded a good forecast skill for the selected typical agricultural droughts (Figure 5). Besides, the nearly perfect forecast of extremum agricultural drought in typical regions (Figure 7) further certified the excellent ability of 3C-vine model.

Heterogeneous topography and anthropogenic activities (e.g., irrigation and urbanization) have certainly impacted precipitation interpolation and soil moisture simulation, which may depart from the actual precipitation or soil moisture conditions, notwithstanding the precipitation of CN05.1 and soil moisture of ERA5 show good performances with respect to drought monitoring and forecasting over China (Wang and Yuan, 2021; Wu et al., 2021a; Xu et al., 2009; Zhang et al., 2021; Zhang et al., 2019). It can also influence the response (propagation) time from meteorological drought to agricultural drought as well as agricultural drought memory and can thus lead to the 3C-vine model falling short in some climate regions. To address this issue, we can comprehensively utilize multiple reanalysis data sets, e.g., the precipitation and soil moisture data in Global Land Data Assimilation System (GLDAS) and ERA5, to reduce the uncertainty resulting from a single data source (Wang and Yuan, 2021; Wu et al., 2021a). Currently, it is a challenge to consider irrigation activities into agricultural drought forecasting, especially at large spatial scales. In addition to antecedent precipitation deficit, air temperature, relative humidity, and evapotranspiration may influence soil moisture budget. Moreover, from the perspective of driving mechanisms, the effect of certain atmospheric circulation anomalies (e.g., El Niño-Southern Oscillation (ENSO), Pacific Decadal

Oscillation (PDO), and North Arctic Oscillation (NAO)) on agricultural drought at regional and global scales can also be considered as predictors (Zhang et al., 2021). Therefore, a more efficient space can be established by leveraging these predictors for forecasting agricultural drought.

In recent years, a myriad of extreme events, such as heatwaves and flash droughts, have swept many regions around the globe. These extreme events have a rapid onset with a few days or weeks and lead to devastating impacts on agricultural production, water resource security, and human well-being (Wang and Yuan, 2021; Yuan et al., 2019; Zscheischler et al., 2020). Therefore, agricultural drought forecasting at finer temporal scales (e.g., weekly) is essential for agricultural managers and policymakers to manage and plan water use. Yet, with limited spatiotemporal resolution and the length of model sample, we temporally have not carried out agricultural drought forecasting at sub-monthly or pentad temporal scales.

The limitation of this study is that we choose a "best" model from two C-vine copula candidate models (i.e., Figure 2) as the ideal forecast. However, as the inherent structural differences (i.e., ordering variables are different), the utilized best model may underestimate the forecast uncertainty (Liu et al., 2021a). Therefore, to reduce the predictive uncertainty and improve the forecast performance, a multi-model combination technique (e.g., Bayesian model averaging (Liu et al., 2021a; Long et al., 2017)) can be considered to merge different C-vine copula candidate models. Moreover, as we only pay attention to the C-vine copulas and several bivariate copula functions, the other D-vine copulas or regular vine copulas, as well as a multitude of bivariate copula families (Sadegh et al., 2017) can be investigated to establish the forecast model for agricultural drought in the next work.

Data availability

The grided monthly precipitation data with a 0.25° spatial resolution was provided by the CN05.1 (http://data.cma.cn) for the period of 1961–2018. The gridded monthly soil moisture data with three soil depths (0–7 cm, 7–28 cm, and 28–100 cm) from the European Center for Medium-Range Weather Forecast (ECMWF) ERA5 reanalysis datasets are available at 1961–1978: https://cds.climate.copernicus.eu/cdsapp#!/dataset/reanalysis-era5-single-levels-monthly-means-preliminary-back-extension?tab=overview and 1979–2018: https://cds.climate.copernicus.eu./cdsapp#!/dataset/reanalysis-era5-single-levels-monthly-means?tab=overview.

Author contribution

Haijiang Wu: Conceptualization, Methodology, Software, Visualization, Writing - original draft. Xiaoling Su: Writing - review & editing, Data curation, Validation, Investigation, Funding acquisition, Supervision, Formal analysis. Vijay P. Singh: Writing - review & editing, Supervision. Te Zhang: Formal analysis, Investigation. Jixia Qi: Data curation, Investigation. Shengzhi Huang: Writing - review & editing, Investigation.

Competing interests

The authors declare that they have no conflict of interest.

Acknowledgments

The authors would like to thank two anonymous reviewers for their constructive comments and suggestions which contributed to improving the quality of the paper. This study was financially supported by the National Natural Science Foundation of China (Grants No. 51879222 and

52079111).

References

Aas, K., and Berg, D.: Models for construction of multivariate dependence – a comparison study, Eur. J. Financ., 15(7-8), 639–659, https://doi.org/10.1080/13518470802588767, 2009.

Aas, K., Czado, C., Frigessi, A., and Bakken, H.: Pair-copula constructions of multiple dependence. Insur. Math. Econ., 44(2), 182–198. https://doi.org/10.1016/j.insmatheco.2007.02.001, 2009.

AghaKouchak, A., Mirchi, A., Madani, K., Di Baldassarre, G., Nazemi, A., Alborzi, A., Anjileli, H., Azarderakhsh, M., Chiang, F., Hassanzadeh, E., Huning, L. S., Mallakpour, I., Martinez, A., Mazdiyasni, O., Moftakhari, H., Norouzi, H., Sadegh, M., Sadeqi, D., Van Loon, A. F., and Wanders, N.: Anthropogenic Drought: Definition, Challenges, and Opportunities, Rev. Geophys., 59(2), e2019RG000683, https://doi.org/10.1029/2019rg000683, 2021.

Bedford, T., and Cooke, R. M.: Vines–A new graphical model for dependent random variables, Ann. Stat., 30(4), 1031–1068, 2002.

Benjamini, Y., and Hochberg, Y.: Controlling the false discovery rate: A practical and powerful approach to multiple testing, J. R. Stat. Soc. Ser. B-Stat. Methodol., 57(1), 289–300, https://doi.org/10.1111/j.2517-6161.1995.tb02031.x, 1995.

Bevacqua, E.: CDVineCopulaConditional: Sampling from conditional C- and D-vine copulas, R package, version 0.1.1, https://CRAN.R-project.org/package=CDVineCopulaConditional, 2017a.

Bevacqua, E., Maraun, D., Hobæk Haff, I., Widmann, M., and Vrac, M.: Multivariate statistical modelling of compound events via pair-copula constructions: analysis of floods in Ravenna (Italy), Hydrol. Earth Syst. Sci., 21(6), 2701–2723, https://doi.org/10.5194/hess-21-2701-

2017, 2017b.

Chen, X., Koenker, R., and Xiao, Z.: Copula-based nonlinear quantile autoregression, Econom. J., 12, S50–S67, https://doi.org/10.1111/j.1368-423X.2008.00274.x, 2009.

Dißmann, J., Brechmann, E. C., Czado, C., and Kurowicka, D.: Selecting and estimating regular vine copulae and application to financial returns, Comput. Stat. Data Anal., 59, 52–69, https://doi.org/10.1016/j.csda.2012.08.010, 2013.

FAO: The impact of disasters and crises on agriculture and food security, Food and Agriculture Organization of the United Nations, Rome, https://doi.org/10.4060/cb3673en, 2021.

Ganguli, P., and Reddy, M. J.: Ensemble prediction of regional droughts using climate inputs and the SVM-copula approach, Hydrol. Process., 28(19), 4989–5009. https://doi.org/10.1002/hyp.9966, 2014.

Genest, C., Rémillard, B., and Beaudoin, D.: Goodness-of-fit tests for copulas: A review and a power study, Insur. Math. Econ., 44(2), 199–213, https://doi.org/10.1016/j.insmatheco.2007.10.005, 2009.

Gringorten, I. I.: A plotting rule for extreme probability paper, J. Geophys. Res., 68(3), 813–814, https://doi.org/10.1029/JZ068i003p00813, 1963.

Hao, Z., Hao, F., Singh, V. P., Sun, A. Y., and Xia, Y.: Probabilistic prediction of hydrologic drought using a conditional probability approach based on the meta-Gaussian model, J. Hydrol., 542, 772–780, https://doi.org/10.1016/j.jhydrol.2016.09.048, 2016.

Hao, Z., Hao, F., Singh, V. P., and Ouyang W.: Quantitative risk assessment of the effects of drought on extreme temperature in eastern China, J. Geophys. Res.-Atmos., 122, 9050–9059, https://doi.org/10.1002/2017JD027030, 2017.

Hao, Z., Hao, F., Singh, V. P., and Zhang, X.: Statistical prediction of the severity of compound dry-hot events based on El Niño-Southern Oscillation, J. Hydrol., 572, 243–250. https://doi.org/10.1016/j.jhydrol.2019.03.001, 2019a.

Hao, Z., Hao, F., Xia, Y., Singh, V. P., and Zhang, X.: A monitoring and prediction system for compound dry and hot events, Environ. Res. Lett., 14(11), 114034, https://doi.org/10.1088/1748-9326/ab4df5, 2019b.

He, L., Hao, X., Li, H., and Han, T.: How Do Extreme Summer Precipitation Events Over Eastern China Subregions Change? Geophys. Res. Lett., 48, e2020GL091849, https://doi.org/10.1029/2020GL091849, 2021.

Hemri, S., Lisniak, D., and Klein, B.: Multivariate postprocessing techniques for probabilistic hydrological forecasting, Water Resour. Res., 51(9), 7436–7451, https://doi.org/10.1002/2014wr016473, 2015.

Joe, H.: Families of m-variate distributions with given margins and m(m−1)/2 bivariate dependence parameters, Institute of Mathematical Statistics Lecture Notes – Monograph Series Distributions with fixed marginals and related topics, 120–141, https://doi.org/10.1214/lnms/1215452614, 1996.

Joe, H.: Dependence modeling with copulas, Chapman and Hall/CRC, 2014.

Lesk, C., Rowhani, P., and Ramankutty, N.: Influence of extreme weather disasters on global crop production, Nature, 529(7584), 84–87, https://doi.org/10.1038/nature16467, 2016.

Liu, B., and Zhu, C.: Extremely Late Onset of the 2018 South China Sea Summer Monsoon Following a La Niña Event: Effects of Triple SST Anomaly Mode in the North Atlantic and a Weaker Mongolian Cyclone, Geophys. Res. Lett., 46(5), 2956–2963, https://doi.org/10.1029/2018gl081718, 2019.

Liu, Z., Cheng, L., Hao, Z., Li, J., Thorstensen, A., and Gao, H.: A Framework for Exploring Joint

Effects of Conditional Factors on Compound Floods, Water Resour. Res., 54(4), 2681–2696, https://doi.org/10.1002/2017wr021662, 2018.

Liu, Z., Cheng, L., Lin, K., and Cai, H.: A hybrid bayesian vine model for water level prediction, Environ. Modell. Softw., 142, 105075, https://doi.org/10.1016/j.envsoft.2021.105075, 2021a.

Liu, Z., Xie, Y., Cheng, L., Lin, K., Tu, X., and Chen, X.: Stability of spatial dependence structure of extreme precipitation and the concurrent risk over a nested basin, J. Hydrol., 602, 126766, https://doi.org/10.1016/j.jhydrol.2021.126766, 2021b.

Long, D., Bai, L., Yan, L., Zhang, C., Yang, W., Lei, H., Quan, J., Meng, X., and Shi, C.: Generation of spatially complete and daily continuous surface soil moisture of high spatial resolution, Remote Sens. Environ., 233, 111364, https://doi.org/10.1016/j.rse.2019.111364, 2019.

Long, D., Pan, Y., Zhou, J., Chen, Y., Hou, X., Hong, Y., Scanlon, B. R., and Longuevergne, L.: Global analysis of spatiotemporal variability in merged total water storage changes using multiple GRACE products and global hydrological models, Remote Sens. Environ., 192, 198–216, https://doi.org/10.1016/j.rse.2017.02.011, 2017.

Lu, Y., Wu, K., Jiang, Y., Guo, Y., and Desneux, N.: Widespread adoption of Bt cotton and insecticide decrease promotes biocontrol services, Nature, 487(7407), 362–365, https://doi.org/10.1038/nature11153, 2012.

Ma, F., Luo, L., Ye, A., and Duan, Q.: Seasonal drought predictability and forecast skill in the semi-arid endorheic Heihe River basin in northwestern China, Hydrol. Earth Syst. Sci., 22, 5697–5709, https://doi.org/10.5194/hess-22-5697-2018, 2018.

Modanesi, S., Massari, C., Camici, S., Brocca, L., and Amarnath, G.: Do Satellite Surface Soil Moisture Observations Better Retain Information About Crop-Yield Variability in Drought Conditions? Water Resour. Res., 56(2), e2019WR025855, https://doi.org/10.1029/2019wr025855, 2020.

Nagler, T., Schepsmeier, U., Stoeber, J., Brechmann, E. C., Graeler, B., Erhardt, T., Almeida, C., Min, A., Czado, C., Hofmann, M., Killiches, M., Joe, H, and Vatter, T,: VineCopula: Statistical Inference of Vine Copulas, R Package Version 2.4.2, https://CRAN.R-project.org/package=VineCopula, 2021.

Nelsen, R. B.: An Introduction to Copulas, 2nd ed., Springer, N. Y., 2013.

Orth, R., and Destouni, G.: Drought reduces blue-water fluxes more strongly than green-water fluxes in Europe, Nat. Commun., 9(1), 3602, https://doi.org/10.1038/s41467-018-06013-7, 2018.

Röthlisberger, M., and Martius, O.: Quantifying the Local Effect of Northern Hemisphere Atmospheric Blocks on the Persistence of Summer Hot and Dry Spells, Geophys. Res. Lett., 46(16), 10101–10111, https://doi.org/10.1029/2019gl083745, 2019.

Sadegh, M., Ragno, E., and AghaKouchak, A.: Multivariate Copula Analysis Toolbox (MvCAT): Describing dependence and underlying uncertainty using a Bayesian framework, Water Resour. Res., 53(6), 5166–5183, https://doi.org/10.1002/2016wr020242, 2017.

Sarhadi, A., Burn, D. H., Concepción Ausín, M., and Wiper, M. P.: Time-varying nonstationary multivariate risk analysis using a dynamic Bayesian copula, Water Resour. Res., 52(3), 2327–2349, https://doi.org/10.1002/2015wr018525, 2016.

Su, B., Huang, J., Fischer, T., Wang, Y., Kundzewicz, Z. W., Zhai, J., Sun, H., Wang, A., Zeng, X., Wang, G., Tao, H., Gemmer, M., Li, X., and Jiang, T.: Drought losses in China might double between the 1.5 degrees C and 2.0 degrees C warming, P. Natl. Acad. Sci. USA, 115(42), 10600–10605, https://doi.org/10.1073/pnas.1802129115, 2018.

Vernieuwe, H., Vandenberghe, S., De Baets, B., and Verhoest, N. E. C.: A continuous rainfall model based on vine copulas, Hydrol. Earth Syst. Sci., 19(6), 2685–2699, https://doi.org/10.5194/hess-19-2685-2015, 2015.

Wang, W., Dong, Z., Lall, U., Dong, N., and Yang, M.: Monthly Streamflow Simulation for the Headwater Catchment of the Yellow River Basin With a Hybrid Statistical-Dynamical Model, Water Resour. Res., 55(9), 7606–7621, https://doi.org/10.1029/2019wr025103, 2019.

Wang, Y., and Yuan, X.: Anthropogenic Speeding Up of South China Flash Droughts as Exemplified by the 2019 Summer-Autumn Transition Season, Geophys. Res. Lett., 48(9), e2020GL091901, https://doi.org/10.1029/2020gl091901, 2021.

Wilks, D. S.: Statistical methods in the atmospheric sciences, Academic Press, 2014.

Wilks, D. S.: “The Stippling Shows Statistically Significant Grid Points”: How Research Results are Routinely Overstated and Overinterpreted, and What to Do about It, B. Am. Meteorol. Soc., 97(12), 2263–2273, https://doi.org/10.1175/bams-d-15-00267.1, 2016.

Wu, H., Su, X., Singh, V. P., Feng, K., and Niu, J.: Agricultural Drought Prediction Based on Conditional Distributions of Vine Copulas, Water Resour. Res., 57(8), e2021WR029562, https://doi.org/10.1029/2021wr029562, 2021a.

Wu, H., Su, X., and Zhang, G.: Prediction of agricultural drought in China based on Meta-Gaussian model, Acta Geogr. Sin., 76(3), 525–538, https://doi.org/10.11821/dlxb202103003, 2021b.

Wu, J., Chen, X., Yu, Z., Yao, H., Li, W., and Zhang, D.: Assessing the impact of human regulations on hydrological drought development and recovery based on a ‘simulated-observed’ comparison of the SWAT model. J. Hydrol., 577, 123990, https://doi.org/10.1016/j.jhydrol.2019.123990, 2019.

Wu, J., Gao, X., Giorgi, F., and Chen, D.: Changes of effective temperature and cold/hot days in late decades over China based on a high resolution gridded observation dataset, Int. J. Climatol., 37, 788–800, https://doi.org/10.1002/joc.5038, 2017.

Xiao, G., Zhao, Z., Liang, L., Meng, F., Wu, W., and Guo, Y.: Improving nitrogen and water use efficiency in a wheat-maize rotation system in the North China Plain using optimized farming practices, Agric. Water Manage., 212, 172–180, https://doi.org/10.1016/j.agwat.2018.09.011, 2019.

Xiong, L., Yu, K.-x., and Gottschalk, L.: Estimation of the distribution of annual runoff from climatic variables using copulas, Water Resour. Res., 50(9), 7134–7152, https://doi.org/10.1002/2013wr015159, 2014.

Xu, L., Chen, N., Chen, Z., Zhang, C., and Yu, H.: Spatiotemporal forecasting in earth system science: Methods, uncertainties, predictability and future directions. Earth-Sci. Rev., 222, 103828, https://doi.org/10.1016/j.earscirev.2021.103828, 2021a.

Xu, Y., Gao, X., Shen, Y., Xu, C., Shi, Y., and Giorgi, F.: A daily temperature dataset over China and its application in validating a RCM simulation, Adv. Atmos. Sci., 26(4), 763–772, https://doi.org/10.1007/s00376-009-9029-z, 2009.

Xu, Y., Zhang, X., Hao, Z., Singh, V. P., and Hao, F.: Characterization of agricultural drought propagation over China based on bivariate probabilistic quantification, J. Hydrol., 598, 126194, https://doi.org/10.1016/j.jhydrol.2021.126194, 2021b.

Yao, N., Li, Y., Lei, T., and Peng, L.: Drought evolution, severity and trends in mainland China over 1961-2013, Sci. Total Environ., 616–617, 73–89, https://doi.org/10.1016/j.scitotenv.2017.10.327, 2018.

Yuan, X., Wang, L., Wu, P., Ji, P., Sheffield, J., and Zhang, M.: Anthropogenic shift towards higher risk of flash drought over China, Nat. Commun., 10(1), 4661, https://doi.org/10.1038/s41467-019-12692-7, 2019.

Zhang, J., Mu, Q., and Huang, J.: Assessing the remotely sensed Drought Severity Index for agricultural drought monitoring and impact analysis in North China, Ecol. Indic., 63, 296–309, https://doi.org/10.1016/j.ecolind.2015.11.062, 2016.

Zhang, L., and Singh, V. P.: Copulas and their applications in water resources engineering, Cambridge University Press, 2019.

Zhang, L., Zhou, T., Chen, X., Wu, P., Christidis, N., and Lott, F. C.: The late spring drought of 2018 in South China, Bull. Amer. Meteorol. Soc., 101(1), S59–S64, https://doi.org/10.1175/BAMS-D-19-0202.1, 2020.

Zhang, Q., Qi, T., Singh, V. P., Chen, Y. D., and Xiao, M.: Regional Frequency Analysis of Droughts in China: A Multivariate Perspective, Water Resour. Manag., 29(6), 1767–1787, https://doi.org/10.1007/s11269-014-0910-x, 2015.

Zhang, Q., Li, Q., Singh, V. P., Shi, P., Huang, Q., and Sun, P.: Nonparametric integrated agrometeorological drought monitoring: Model development and application, J. Geophys. Res.-Atmos., 123, 73–88, https://doi.org/10.1002/2017JD027448, 2018.

Zhang, Q., Yu, H., Sun, P., Singh, V. P., and Shi, P.: Multisource data based agricultural drought monitoring and agricultural loss in China, Glob. Planet. Change, 172, 298–306, https://doi.org/10.1016/j.gloplacha.2018.10.017, 2019.

Zhang, T., Su, X., and Feng, K.: The development of a novel nonstationary meteorological and hydrological drought index using the climatic and anthropogenic indices as covariates, Sci. Total Environ., 786, 147385, https://doi.org/10.1016/j.scitotenv.2021.147385, 2021.

Zhang, X., Su, Z., Lv, J., Liu, W., Ma, M., Peng, J., and Leng, G.: A Set of Satellite-Based Near Real-Time Meteorological Drought Monitoring Data over China, Remote Sens., 11(4), 453, https://doi.org/10.3390/rs11040453, 2019.

Zhang, Y., Hao, Z., Feng, S., Zhang, X., Xu, Y., and Hao, F.: Agricultural drought prediction in China based on drought propagation and large-scale drivers, Agric. Water Manage., 255, 107028, https://doi.org/10.1016/j.agwat.2021.107028, 2021.

Zhang, Y., Wang, Z., Sha, S., and Feng, J.: Drought Events and Its Causes in Summer of 2018 in China. J. Arid Meteoro., 36(5), 884–892, https://doi.org/10.11755/j.issn.1006-7639(2018)-05-0884, 2018.

Zhao, S.: A new scheme for comprehensive physical regionalization in China, Acta Geogr. Sin., 38(1), 1–10, 1983.

Zhou, S., Williams, A. P., Berg, A. M., Cook, B. I., Zhang, Y., Hagemann, S., Lorenz, R., Seneviratne, S. I., and Gentine, P.: Land-atmosphere feedbacks exacerbate concurrent soil drought and atmospheric aridity, P. Natl. Acad. Sci. USA, 116(38), 18848–18853, https://doi.org/10.1073/pnas.1904955116, 2019.

Zscheischler, J., Martius, O., Westra, S., Bevacqua, E., Raymond, C., Horton, R. M., van den Hurk, B., AghaKouchak, A., Jézéquel, A., Mahecha, M. D., Maraun, D., Ramos, A. M., Ridder, N. N., Thiery, W., and Vignotto, E.: A typology of compound weather and climate events, Nature Reviews Earth & Environment, 1(7), 333–347, https://doi.org/10.1038/s43017-020-0060-z, 2020.

Figure Captions

Figure 1. Seven sub-climate regions division over China. The specific information of climate regions D1–D7 is listed at the left-bottom in the panel.

Figure 2. Different schematic (two types) of C-vine copulas under three-dimensional scenarios. For the first type (a), the ordering variables are y_1, y_2, and y_3, while for the second type (b) that are y_2, y_1, and y_3. $C_{12}(C_{21})$, $C_{13}(C_{23})$, and $C_{23|1}(C_{13|2})$ denotes bivariate copulas with parameters θ_{11}, θ_{12}, and θ_{21}, respectively. Here, θ_{ij} signifies the parameters of the j-th edge with respect to the i-th tree. $G(\bullet|\bullet)$ denote conditional distribution functions.

Figure 3. Flowchart of agricultural drought forecasting based on canonical vine copulas (3C-vine) and meta-Gaussian (MG) model under three-dimensional scenarios. Here, t denotes the target month (e.g., August); i signifies the lead times (1–3-months)); LOOCV is the abbreviation of leave-one-out cross validation; $y_1^{-yr}(y_2^{-yr})$ indicates the series after removing a sample $(y_1^{yr}(y_2^{yr}))$ for a specific year; and y_3^{yr} is the agricultural drought forecast value for the target month of a specific year. Note that the optimal tree structure (*i* or *ii* on the right-hand side of this figure) is selected based on AIC to forecast agricultural drought.

Figure 4. Spatial patterns of 1–3-months lag Kendall's correlation coefficient (τ_k) between SPI_{t-i} and SSI_t (t denotes August, and i is 1–3-month lag time) (top row), as well as SSI_{t-i} and SSI_t (bottom row) for August during 1961–2018 over China. Note the stippling indicates where τ_k is at a 0.05 significance level, which is corrected via the false discovery rate (FDR) of 0.1.

Figure 5. Forecast performance based on (a–c) ΔNSE (difference of NSE between 3C-vine and MG

models, NSE_{3C}–NSE_{MG}), (d–f) ΔR^2 (R^2_{3C}–R^2_{MG}), and (g–i) $\Delta RMSE$ ($RMSE_{3C}$–$RMSE_{MG}$) for the 1–3-month leads of August during 1961–2018 over China. The corresponding boxplots of (j) ΔNSE, (k) ΔR^2, and (l) $\Delta RMSE$ relative to a threshold of 0 (horizontal black dash line) for agricultural drought forecast in August under 1–3-month leads in climate regions D1–D7 over China. The percentage of $\Delta NSE > 0$, $\Delta R^2 > 0$, and $\Delta RMSE < 0$ is listed in the left-bottom of corresponding sub-figure, respectively.

Figure 6. SSI observations in August of 2018 (a) as well as the corresponding SSI forecasts under 1–3-month lead times utilizing 3C-vine model (b–d) and MG model (e–g) over China. The black rectangle boxes (as shown in b) denote the typical regions (corresponding to signify D1S–D7S) selected in climate regions D1–D7.

Figure 7. Probability density function (PDF) curve of (a and c) minimum and (b and d) maximum SSI under 1–3-month lead times for August and July during the 1961–2018 period over seven selected typical regions in climate regions D1–D7 (i.e., these black rectangle boxes in Figure 6b correspond to signify D1S–D7S, respectively). Black dash line and text indicate the minimum and maximum observations of SSI in August and July over D1S–D7S. These texts with red (green), blue (yellow), and cyan (coral) colors of left (right) in each sub-figure are SSI forecasts under 1–3-month lead times of August or July via 3C-vine model (MG model), which correspond to the abscissa projected by the peak point of each PDF.

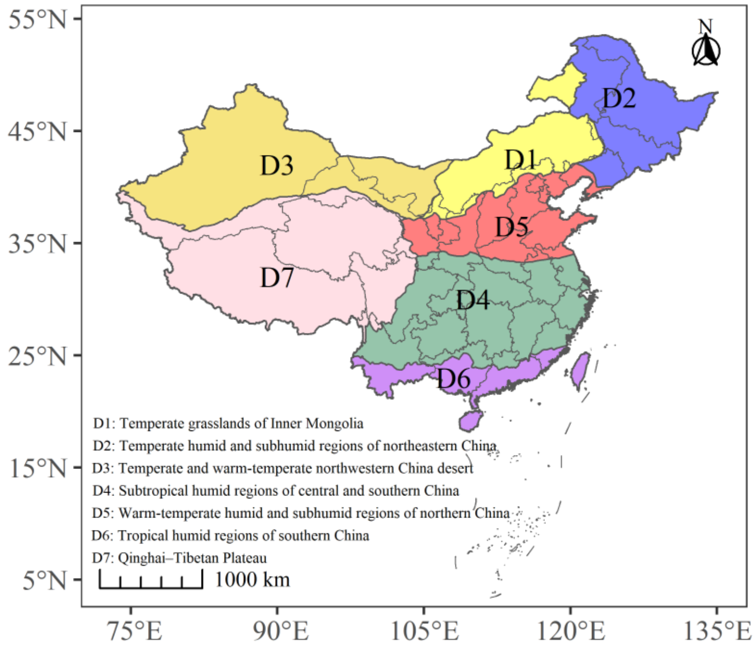

Figure 1. Seven sub-climate regions division over China. The specific information of climate regions D1–D7 is listed at the left-bottom in the panel.

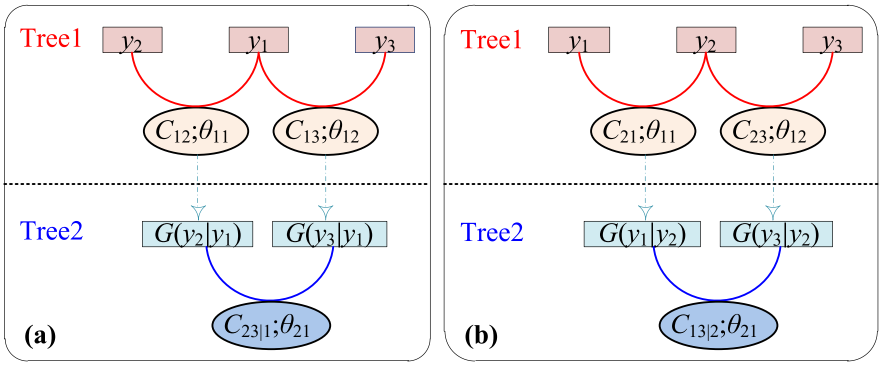

Figure 2. Different schematic (two types) of C-vine copulas under three-dimensional scenarios. For the first type (a), the ordering variables are y_1, y_2, and y_3, while for the second type (b) that are y_2, y_1, and y_3. C_{12}(C_{21}), C_{13}(C_{23}), and $C_{23|1}$($C_{13|2}$) denotes bivariate copulas with parameters θ_{11}, θ_{12}, and θ_{21}, respectively. Here, θ_{ij} signifies the parameters of the j-th edge with respect to the i-th tree. $G(\bullet|\bullet)$ denote conditional distribution functions.

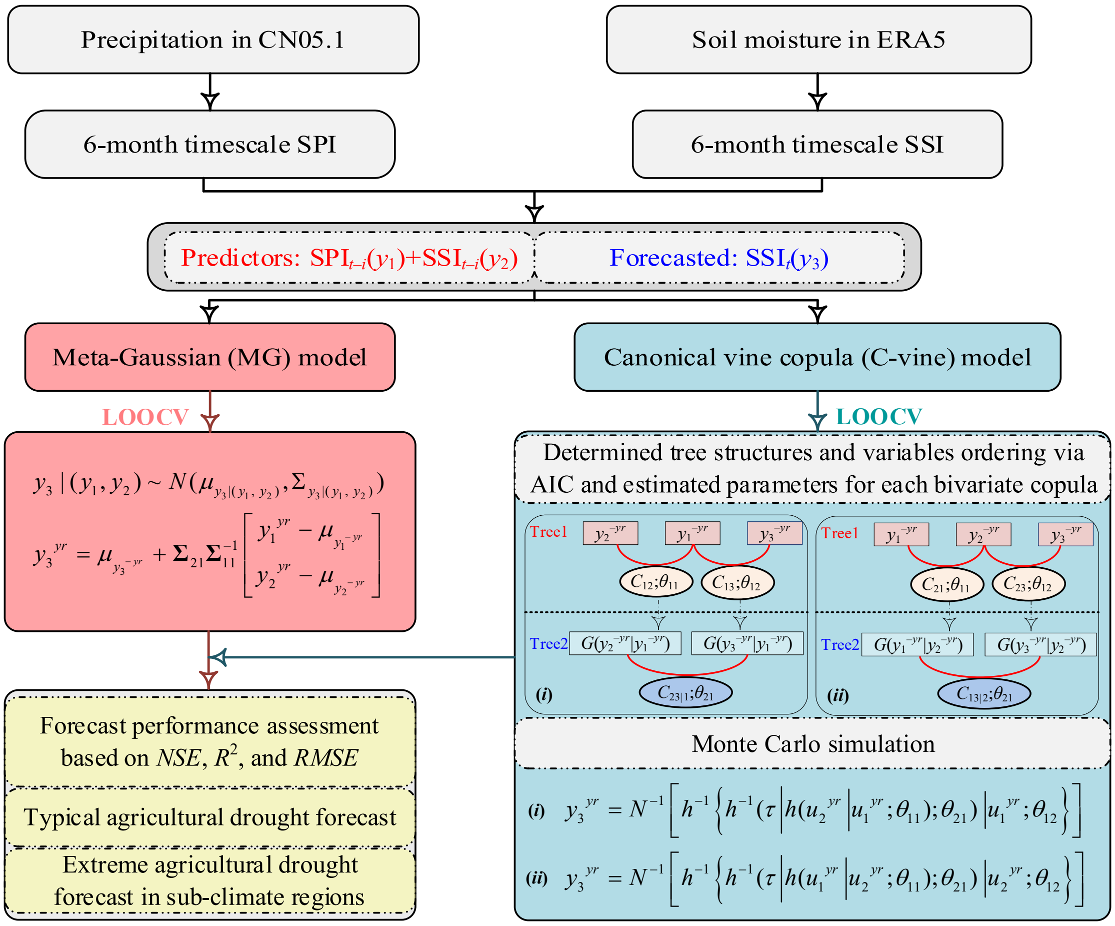

Figure 3. Flowchart of agricultural drought forecasting based on canonical vine copulas (3C-vine) and meta-Gaussian (MG) model under three-dimensional scenarios. Here, *t* denotes the target month (e.g., August); *i* signifies the lead times (1–3-months)); LOOCV is the abbreviation of leave-one-out cross validation; $y_1^{-yr}(y_2^{-yr})$ indicates the series after removing a sample $(y_1^{yr}(y_2^{yr}))$ for a specific year; and y_3^{yr} is the agricultural drought forecast value for the target month of a specific year. Note that the optimal tree structure (*i* or *ii* on the right-hand side of this figure) is selected based on AIC to forecast agricultural drought.

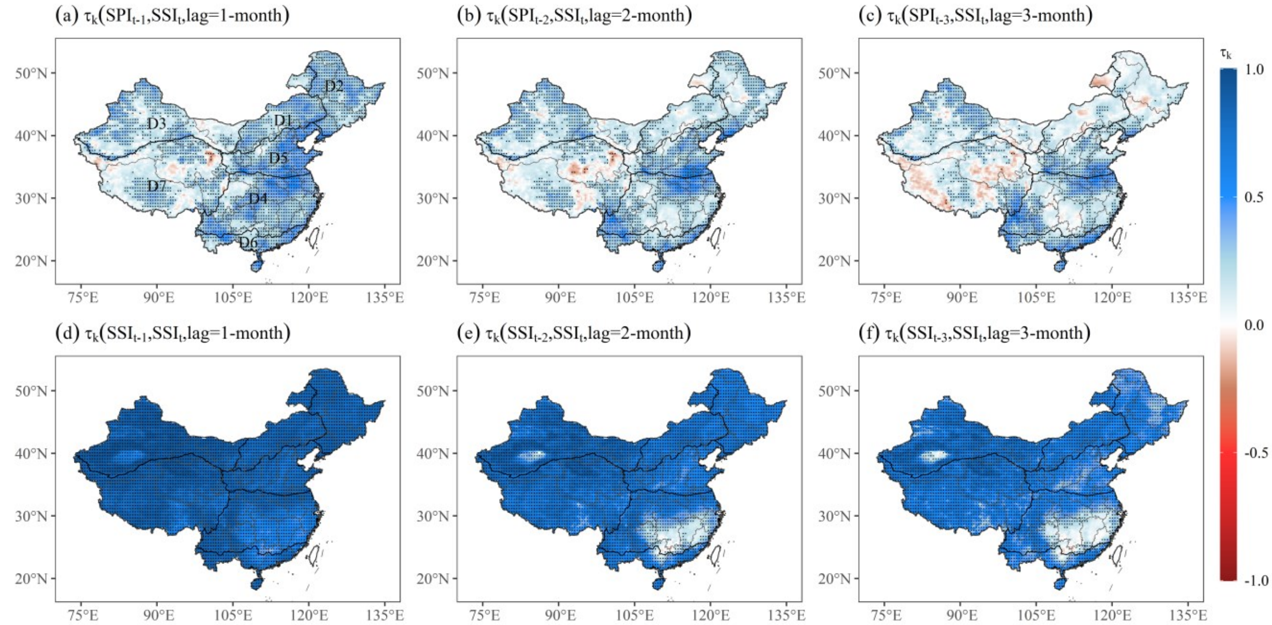

Figure 4. Spatial patterns of 1–3-months lag Kendall's correlation coefficient (τ_k) between SPI_{t-i} and SSI_t (t denotes August, and i is 1–3-month lag time) (top row), as well as SSI_{t-i} and SSI_t (bottom row) for August during 1961–2018 over China. Note the stippling indicates where τ_k is at a 0.05 significance level, which is corrected via the false discovery rate (FDR) of 0.1.

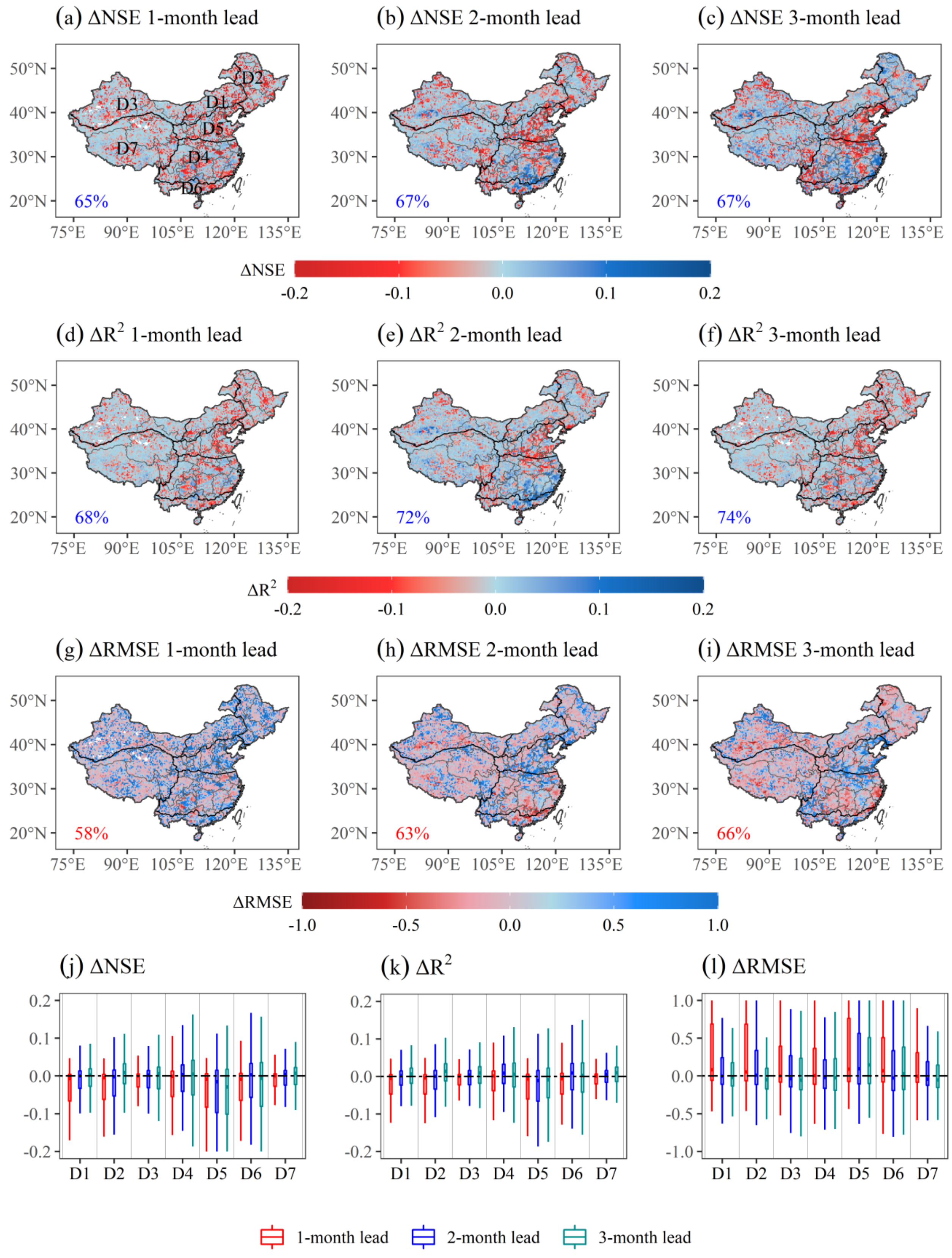

Figure 5. Forecast performance based on (a–c) Δ*NSE* (difference of *NSE* between 3C-vine and MG models, $NSE_{3C}–NSE_{MG}$), (d–f) ΔR^2 ($R^2_{3C}–R^2_{MG}$), and (g–i) $\Delta RMSE$ ($RMSE_{3C}–RMSE_{MG}$) for the

1–3-month leads of August during 1961–2018 over China. The corresponding boxplots of (j) ΔNSE, (k) ΔR^2, and (l) $\Delta RMSE$ relative to a threshold of 0 (horizontal black dash line) for agricultural drought forecast in August under 1–3-month leads in climate regions D1–D7 over China. The percentage of $\Delta NSE > 0$, $\Delta R^2 > 0$, and $\Delta RMSE < 0$ is listed in the left-bottom of corresponding sub-figure, respectively.

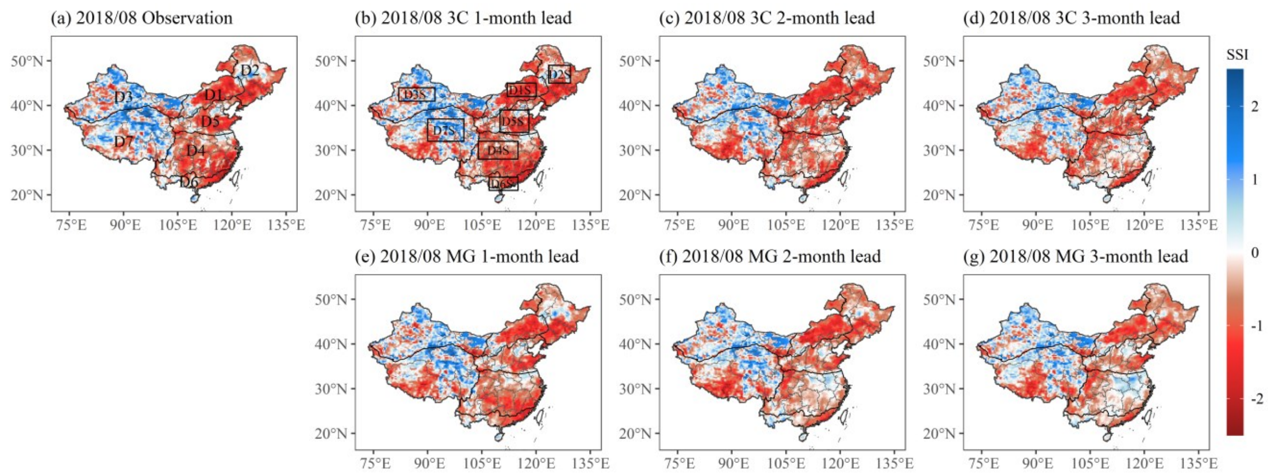

Figure 6. SSI observations in August of 2018 (a) as well as the corresponding SSI forecasts under 1–3-month lead times utilizing 3C-vine model (b–d) and MG model (e–g) over China. The black rectangle boxes (as shown in b) denote the typical regions (corresponding to signify D1S–D7S) selected in climate regions D1–D7.

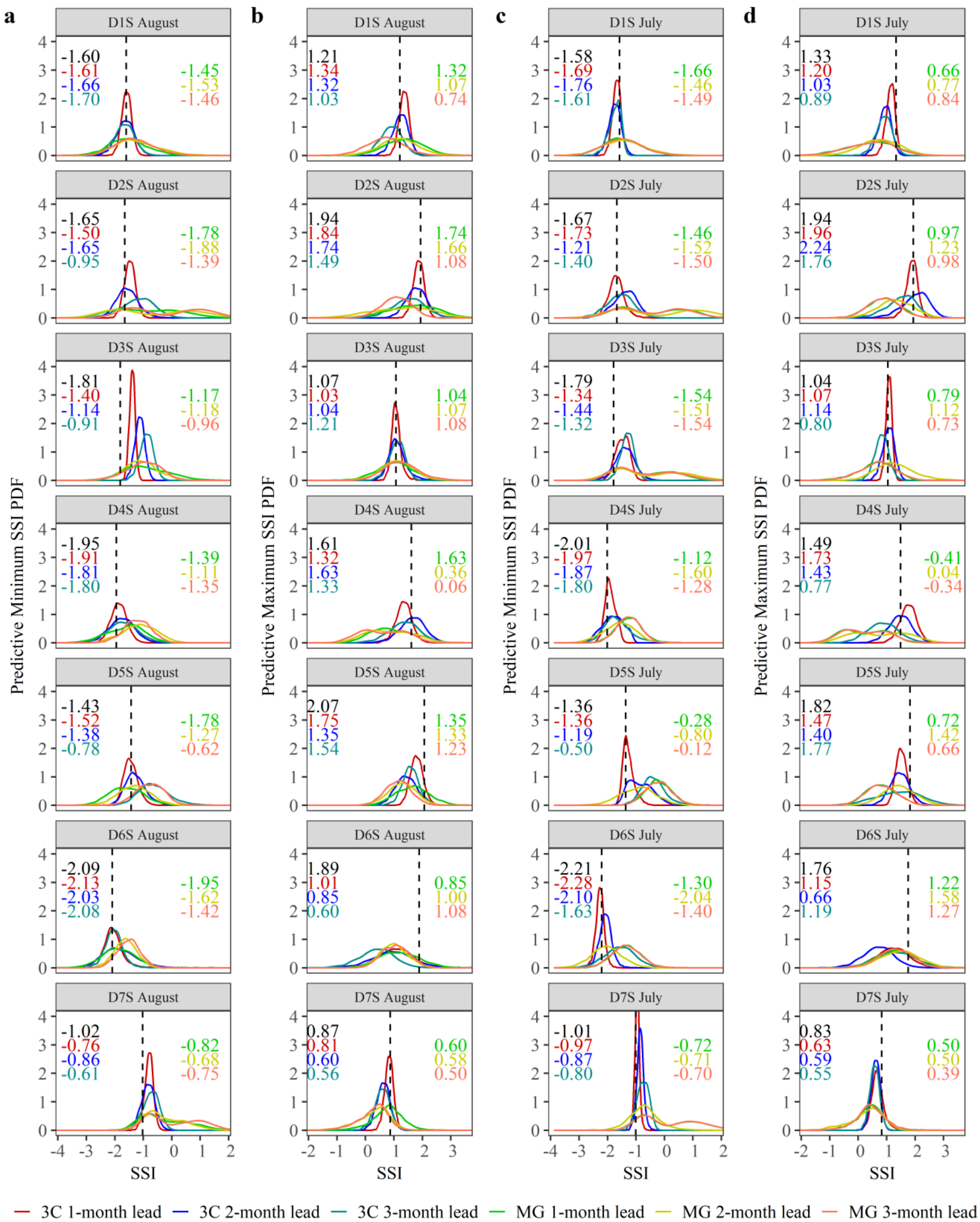

Figure 7. Probability density function (PDF) curve of (a and c) minimum and (b and d) maximum SSI under 1–3-month lead times for August and July during the 1961–2018 period over seven selected typical regions in climate regions D1–D7 (i.e., these black rectangle boxes in Figure 6b

correspond to signify D1S–D7S, respectively). Black dash line and text indicate the minimum and maximum observations of SSI in August and July over D1S–D7S. These texts with red (green), blue (yellow), and cyan (coral) colors of left (right) in each sub-figure are SSI forecasts under 1–3-month lead times of August or July via 3C-vine model (MG model), which correspond to the abscissa projected by the peak point of each PDF.